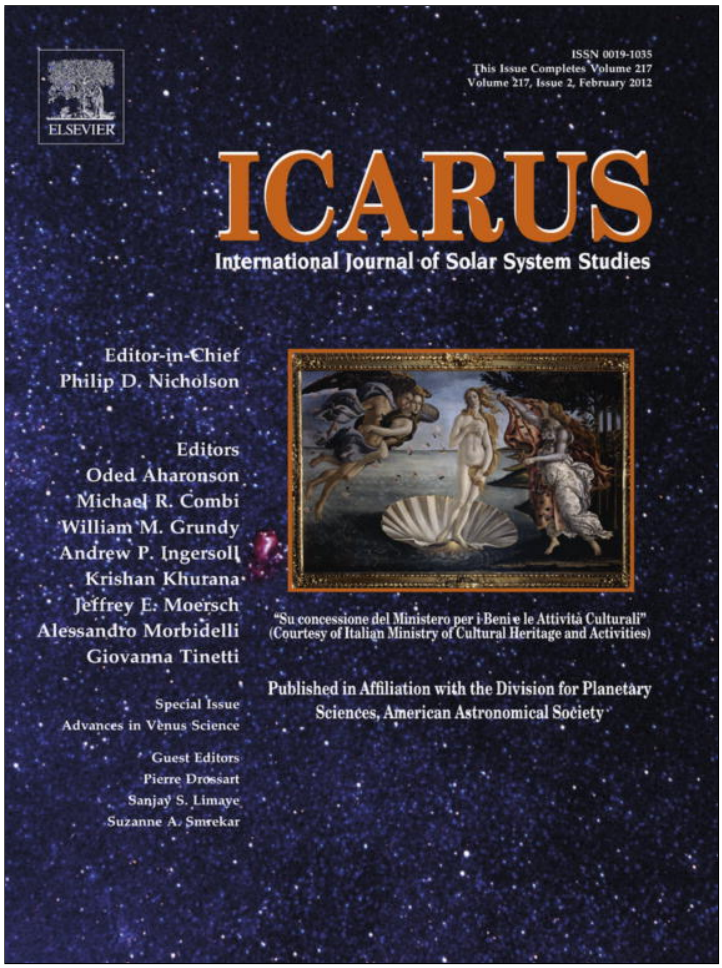

Icarus 217 (2012) 484–498

Contents lists available at SciVerse ScienceDirect

Icarus

journal homepage: www.elsevier.com/locate/icarus

Coupling the atmosphere with interior dynamics: Implications for the resurfacing of Venus

L. Noack [a,*], D. Breuer [b], T. Spohn [b]

[a] Joint Planetary Interior Physics Research Group of Münster University and the Institute of Planetary Research, DLR Berlin, Rutherfordstraße 2, 12489 Berlin, Germany
[b] Institute of Planetary Research, German Aerospace Center (DLR), Rutherfordstraße 2, 12489 Berlin, Germany

ARTICLE INFO

Article history:
Available online 10 September 2011

Keywords:
Venus
Venus, Atmosphere
Venus, Interior
Atmospheres, Evolution
Thermal histories

ABSTRACT

We calculated 2D and 3D mantle convection models for Venus using digitized atmosphere temperatures from the model of Bullock and Grinspoon (Bullock, M.A., Grinspoon, D.H. [2001]. Icarus 150, 19–37) to study the interaction between interior dynamics and atmosphere thermal evolution. The coupling between atmosphere and interior occurs through mantle degassing and the effect of varying concentrations of the greenhouse gas H_2O on the surface temperature. Exospheric loss of hydrogen to space is accounted for as a H_2O sink. The surface temperature enters the mantle convection model as a boundary condition.

Our results suggest a self-consistent feedback mechanism between the interior and the atmosphere resulting in spatial–temporal surface renewal. Greenhouse warming of the atmosphere results in an increase in the surface temperature. Whenever the surface temperature reaches a critical value, the viscosity difference across the lithosphere becomes smaller than about 10^5 and the surface becomes locally mobile. The critical surface temperature depends on the activation energy for mantle creep, the stress exponent in the non-Newtonian mantle rheology law, and the mantle temperature. Surface renewal together with surface lava flow may explain why the surface of Venus is young on average, i.e. not older than a few hundred million years.

The mobilization of the near-surface lithosphere increases the rate of heat removal from the mantle and thereby the interior cooling rate. The enhanced cooling results in a reduction of the water outgassing rates. As a consequence of decreasing water concentrations in the atmosphere, the surface temperature decreases. Our model calculations suggest that Venus should have been geologically active until recently. This is in agreement with several lines of observational evidence from thermal emissivity measurements and crater distribution analyses.

1. Introduction

The thermal evolution of a terrestrial planet involves heat transfer from the interior by convection (Schubert et al., 2002; Turcotte and Schubert, 2002), volcanism, and chemical differentiation. On one-plate planets like Mars, convection takes place below a stagnant upper layer and most of the heat is transported via conduction through this layer. On Earth, convection incorporates the surface layers through plate tectonics which results in the interior being cooled more efficiently than in the case of stagnant lid convection (e.g. Schubert et al., 2002). Plate tectonics can be regarded as a specific form of mobile lid convection where the mobile lid being mechanically stiff moves across the surface of the mantle as (several, distinct) plates. The climatic evolution of a planet is mainly controlled by the solar flux and the amount of greenhouse gases in the atmosphere. The latter may change significantly over time as greenhouse gases are released into the atmosphere by volcanic outgassing, leading to an increase in surface temperature. High surface temperatures may reduce the plate-like behaviour of the lithosphere – by making it more ductile – as was suggested for Venus by Lenardic et al. (2008), which in turn influences the climate since plate tectonics can recycle atmospheric CO_2 into the mantle. Higher surface temperatures may also result in an increase in mantle temperature and a corresponding increase in partial-melting and outgassing rates.

Phillips et al. (2001) investigated the coupling effect of the surface temperature on mantle dynamics for Venus by using simple parameterized convection models. They considered the outgassing of the greenhouse gas H_2O using a gray atmosphere model (Wildt, 1966; Sagan, 1969). Their model revealed a positive feedback mechanism: an increase in surface temperature leads to an increase in partial melting and hence an increase in atmospheric density and surface temperature. This triggers a positive runaway effect, which destabilizes the climate of the planet. The mechanism is illustrated in Fig. 1.

* Corresponding author.
E-mail address: lena.noack@dlr.de (L. Noack).

0019-1035/$ - see front matter © 2011 Elsevier Inc. All rights reserved.
doi:10.1016/j.icarus.2011.08.026

Parameterized models are limited by their inability to adapt the convective regime (e.g. stagnant lid, mobile lid, plate tectonics) to changing boundary conditions such as the surface temperature, and because there is no lateral variation e.g. in lid thickness or convective stress. Whereas average lid thickness is self-consistently calculated during a parameterized thermal evolution calculation as long as the surface is in a stagnant-lid regime, transitions from a stagnant-lid to a locally mobile regime cannot be simulated. This limitation does not exist in 2D or 3D interior models which simulate fully convective mantle behaviour, so that the feedback mechanism might be different than illustrated in Fig. 1.

For the work presented in this paper we use the spherical convection simulation code GAIA (Hüttig and Stemmer, 2008) to which we added an atmosphere module that uses the digitized average surface temperature from Bullock and Grinspoon (2001) (their Fig. 6) as a function of the water vapour concentration in the atmosphere. We modify these surface temperatures for varying solar luminosities following Gough (1981). It is widely accepted that the solar luminosity has increased by about 40% in the past 4.5 Gyr. The concentration of water in the atmosphere is calculated from the mantle outgassing rate while employing observed exospheric loss rates. The influence of mantle outgassing on the atmosphere as well as the feedback effect on the interior through the surface temperature can then be calculated self-consistently.

Venus is a particularly good candidate to which to apply such a model. Venus today has a surface temperature of about 740 K, which is too high for liquid water to exist on the surface. The temperature is caused mainly by the greenhouse gases CO_2 and H_2O (Lewis, 2004; Grinspoon, 1993; Bullock and Grinspoon, 2001) of which H_2O is particularly effective with relatively small variations in concentrations having significant effects on the temperature as demonstrated by the models of Pollack (1969), Pollack et al. (1980) and Bullock and Grinspoon (2001).

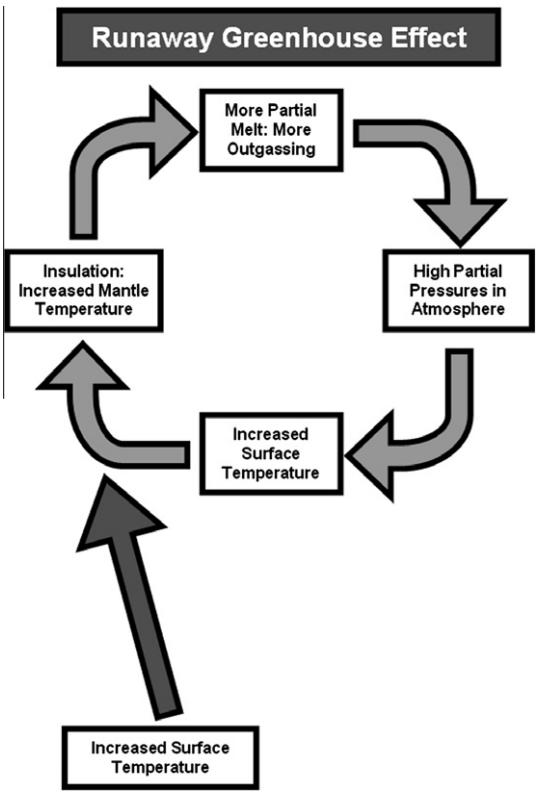

Fig. 1. Sketch illustrating the runaway greenhouse effect on a planet like Venus according to Phillips et al. (2001). Increases in surface temperature (e.g. due to outgassing) reduce mantle heat flux and increase mantle temperatures and melting rates, thus further increasing the surface temperature.

Another singular characteristic of Venus is the age of its surface, which is 300 Myr to 1 Gyr on average (McKinnon et al., 1997; Schaber et al., 1992; Strom et al., 1994). Romeo and Turcotte (2010) investigated the number and distribution of impact craters as well as the proportion of modified craters, concluding that these might indicate a catastrophic resurfacing event. In their model they assumed a gradual decrease in volcanic activity, so that about 40% of the surface would have been resurfaced in the last 750 Myr. Other studies (Schaber et al., 1992; Strom et al., 1994) identify a catastrophic resurfacing event, followed by much-reduced resurfacing activity.

For such a (possibly episodic) catastrophic global resurfacing event, several geodynamical explanations have been proposed so far. The event could have been exclusively magmatic (Reese et al., 1999), or caused by lithosphere thickening leading to episodic subduction and mantle overturn (Schubert et al., 1997; Fowler and O'Brian, 1996; Turcotte et al., 1999; Turcotte, 1993), or by a depleted layer on top of the mantle sinking down due to negative thermal buoyancy (Parmentier and Hess, 1992). Another explanation considers phase transitions in the mantle, which might lead to prolonged layered convection. At some point, however, a transition from layered to whole-mantle convection might occur, giving rise to a catastrophic resurfacing event (Steinbach et al., 1993). Further potential explanations include a cessation of plate tectonics 500 Myr ago (Schubert et al., 1997, 2002) or even episodic brittle mobilization due to a higher friction coefficient compared to Earth (Moresi and Solomatov, 1998; Stein et al., 2010). Basilevsky and Head (1998) explain geological features at the surface by compression and tension caused by variations in surface temperature over several hundred Myr but do not entirely rule out plate tectonics to be the cause of these features at an earlier stage of evolution.

Even on Earth, where plate tectonics is active, a large proportion of the surface – the continental crust – is several billion years old. We know from Magellan data that on Venus, too, some surface features (tessera terrains (Ivanov and Head, 1996)) seem to be much older than the mean values mentioned above (e.g. Hansen and López, 2010) and may even be comparable in age to Earth's continental crust. These investigations support another resurfacing history in which small patches are resurfaced at different times (Phillips et al., 1992; Phillips and Hansen, 1998; Guest and Stofan, 1999); features like coronae and plains basins seem to be much younger than the crustal plateaus. Consequently, catastrophic resurfacing seems less likely but cannot be ruled out. However, as these areas are quite small it is not possible to estimate their age reasonably by the crater counting method (Hauck et al., 1998; Hansen, 2000).

Smrekar et al. (2010) interpreted VIRTIS emissivity data as indicating recent volcanism on Venus and argued for gradual resurfacing. Recent volcanism in the last tens of Myr is also needed to explain the high concentration of SO_2 in the atmosphere (Bullock and Grinspoon, 2001). Stofan et al. (2005) conclude in their study that two thirds of the venusian surface is covered by volcanic material (e.g. coronae or large volcanoes) while one third has no identifiable source. These plains are interpreted as having a volcanic source but might as well be of different (unknown) origin.

Today, a highly sluggish or stagnant-lid regime is thought to prevail on Venus (Schubert et al., 1997; Nimmo and McKenzie, 1998). When surface temperatures were much higher in the past, Venus might have had a mobile surface, however. Reese et al. (1999) estimated that surface temperatures must exceed a critical value of about 1000 K to allow a transformation from a stagnant-lid to a global mobile regime. Higher surface temperatures than today – in the range of 850–1000 K – have been suggested by Phillips and Hansen (1998) and Ruiz (2007) to explain the formation of

ribbon terrains, assuming a dry diabase rheology. It should be mentioned, however, that results may be different when assuming a more felsic composition instead (Mueller et al., 2008). When trying to understand the thermal evolution of Venus it is hence crucial to adapt models of the interior dynamics to varying surface temperatures.

Instead of using fixed surface temperatures for our 2D and 3D spherical mantle convection model, we varied the surface temperature using the results of Bullock and Grinspoon (2001) adapted for varying values of the solar luminosity (Gough, 1981). We thus self-consistently obtain local resurfacing events (including the recycling of surface material back into the interior due to a local mobile regime) caused by elevated surface temperatures during Venus' evolution. This is a possible explanation of the young average age of the surface, which is also supported by the recent observations of Venus Express (Smrekar et al., 2010). We obtain widespread resurfacing by volcanism and local surface mobilization and decreasing gradual resurfacing after that. Furthermore, we obtain small patches of the surface older than 1 Gyr (up to more than 3 Gyr) as suggested by Hansen and López (2010) and recent resurfacing as suggested by Smrekar et al. (2010). The average surface age is up to some hundreds of million years in our models but greatly depends on the parameter set used. Enhanced mantle cooling by surface mobilization causes a gradual decrease of volcanism while Venus' mantle has been partially depleted of volatiles. Hence, present day volcanism could still act as an H_2O source which would explain the high amount of water vapour (and other greenhouse gases) in the present-day atmosphere, see also Taylor and Grinspoon (2009). The present paper provides an explanation why resurfacing due to volcanism and mobilization decreases gradually over time and acts locally.

2. Numerical model

Mantle dynamics is treated by simulating convection in a spherical shell, where we assume an olivine-dominated rheology and an iron-rich core thermally coupled to the mantle shell. We use a 2D/3D spherical simulation code that includes partial melting (Plesa and Breuer, 2010) to model mantle degassing; the formation of a chemically distinct crust is, however, neglected.

Heat produced in the mantle by radioactive decay and primordial heat stored in the interior is transported to the surface by convection. Rising mantle material melts in the upper mantle by decompression melting. This melt is enriched with H_2O volatiles. Once it has risen to the surface, the greenhouse gases are released into the atmosphere, causing increases in density, partial pressures, and surface temperatures. No recycling of volatiles is considered in the model. The calculation of the amount of partial melt and of volatiles released into the atmosphere is described in Section 2.2.

We compare two model setups after Phillips et al. (2001), a coupled version and an uncoupled model. In the coupled model (see also Noack, 2009), the surface temperature from the atmosphere model is used as a thermal boundary condition for the mantle convection model. In the uncoupled model, atmospheric surface temperatures are derived but the surface temperature in the mantle convection model is taken constant at 737 K. Thereby, it can be investigated how changes in the atmosphere temperature affect interior dynamics and vice versa.

2.1. Mantle convection model

We use the standard hydrodynamic description of mantle flow with partial differential equations that are solved with the aid of the spherical code GAIA in a 2D/3D geometry (Hüttig and Stemmer, 2008) by means of the finite-volume method. The non-dimensional conservation equations of mass, momentum and energy in the extended Boussinesq approximation (Ita and King, 1994) are

$$\nabla \cdot v' = 0 \tag{1}$$

$$\nabla \cdot [\eta'(\nabla v' + (\nabla v')^T)] + RaT' e_r - \nabla p' = 0 \tag{2}$$

$$\frac{\partial T'}{\partial t'} + v'\nabla T' + Di(T' + T'_0)v'_r = \nabla^2 T' + \frac{Ra_Q(t)}{Ra} + \frac{Di}{2Ra}\eta'(\nabla v' + \nabla v'^T)^2, \tag{3}$$

with the non-dimensional velocity represented by v', radial velocity by v'_r, the viscosity by η', the radial unity vector by e_r, the Rayleigh number by Ra, the internal Rayleigh number by Ra_Q, temperature by T', the surface temperature by T'_0, the dynamic pressure by p', the time by t' and the dissipation number by $Di = \alpha_m g D/C_{p,m}$. The dissipation number depends on thermal expansivity α_m, gravity acceleration g, mantle thickness D, and heat capacity of the mantle $C_{p,m}$, and is assumed to be constant in the mantle.

We use the standard non-dimensionalization factors and Rayleigh numbers employed in mantle convection simulations (e.g. Christensen, 1984):

$$\begin{aligned} T' &= \frac{T - T_0}{\Delta T}, \quad T'_0 = \frac{T_0}{\Delta T}, \quad z' = \frac{z}{D}, \quad v' = \frac{v}{\kappa_m/D}, \\ t' &= \frac{t}{D^2/\kappa_m}, \quad p' = \frac{p}{\eta_{ref}\kappa_m/D^2}, \quad \eta' = \frac{\eta}{\eta_{ref}}, \\ Ra &= \frac{\rho_m g \alpha_m \Delta T D^3}{\kappa_m \eta_{ref}}, \quad Ra_Q(t) = \frac{\rho_m g \alpha_m H(t) D^5}{k_m \kappa_m \eta_{ref}} \end{aligned} \tag{4}$$

where ΔT is the temperature contrast across the mantle, z the depth, κ_m the thermal diffusivity in the mantle, and ρ_m the mantle density. k_m represents thermal conductivity and H the volumetric rate of heat generation by radioactive decay (see Eq. (8)).

The viscosity of a non-Newtonian fluid is defined using Arrhenius' formula (e.g. van Hunen et al., 2004).

$$\eta = A^{-1/n}\dot{\varepsilon}^{(1-n)/n}\exp\left(\frac{E + p_h V}{nRT}\right) \tag{5}$$

Viscosity depends on an experimental prefactor A, the strain rate $\dot{\varepsilon}$, the viscosity stress exponent n, the activation energy E and activation volume V, the universal gas constant R, the temperature T, and the hydrostatic pressure p_h, which increases linearly with the depth z,

$$p_h = \rho_m g z \tag{6}$$

We assume a dry non-Newtonian rheology (Karato and Wu, 1993) and use the approach of Christensen (1984) to approximate non-Newtonian viscosity by applying Newton's linear law with constant reference prefactors and dividing the activation enthalpy by the stress exponent n (compare Eq. (5)). The non-dimensional parameters for viscosity are:

$$E' = \frac{E}{R\Delta T}, \quad V' = \frac{V\rho_m g D}{R\Delta T}, \quad \dot{\varepsilon}'_{ref} = \frac{\dot{\varepsilon}_{ref}}{\kappa_m/D^2} \tag{7}$$

We define a reference viscosity of 10^{21} Pa s at a reference temperature of 1600 K and a reference depth of 100 km (Karato and Wu, 1993). We assume a constant reference strain rate of 10^{-16} 1/s to be used in Eq. (5) and for the definition of our reference viscosity.

The thermal evolution of Venus is simulated for 4.5 Gyr, during which the heat production rate decays over time, depending on the decay constant λ (Schubert et al., 2002),

$$H(t) = H_0 \exp(-\lambda t) \tag{8}$$

The core cools depending on the average heat flux q_{CMB} at the CMB,

$$\frac{\partial T_{CMB}}{\partial t} = -\frac{q_{CMB} A_c}{\rho_c C_{p,c} V_c}; \quad q_{CMB} = k_m \frac{\partial \overline{T}}{\partial z}\bigg|_{CMB}. \tag{9}$$

Here, A_c is the surface area and V_c the volume of the core; ρ_c is the core density and $C_{p,c}$ the specific heat capacity of the core. The average core heat flux q_{CMB} is calculated by laterally averaging the local heat flux into the mantle at the core–mantle boundary.

We use free-slip boundary conditions at the core–mantle boundary and at the surface. The initial temperature profile is defined on the basis of the initial mantle temperature $T_{m,ini}$, see Table 2, and two boundary layers (Buske, 2006). The surface temperature of the initial profile (non-dimensional $T' = 0$) depends on solar luminosity and initial concentration of water in the atmosphere. The initial temperature profile increases in the upper 20% of the mantle to the initial mantle temperature in a sine function. In the lowermost 30% of the mantle, the temperature increases further, again in a sine function, until the core–mantle temperature of initially 4000 K ($T' = 1$) is reached. In our 3D model we use a radial resolution of 32 shells with 1024 points per shell; the 2D model uses 64 shells of 584 points each.

We define the surface as locally mobilized if convective heat transport from the mantle to the surface is more efficient than heat conduction. We use the Peclet number, *Pe*, defined as the ratio between the energy transported by convection and diffusion,

$$Pe := \frac{vD}{\kappa} \approx \frac{|\vec{v} \cdot \nabla T|}{|\kappa \nabla^2 T|} \tag{10}$$

If the Peclet number is greater than one, local mobilization of the surface occurs. For Venus, a Peclet number of one corresponds to a convective velocity of only 10^{-5} m/yr. For Peclet numbers around one the flow is highly sluggish. To distinguish between the sluggish and the mobile regime, we assume for our investigations the transition to occur at a Peclet number of 100 (corresponding to 1 mm/yr).

To determine the effectiveness of surface recycling, we trace surface mobilization using a double-diffusive solver. We consider a near-surface layer with a thickness of 50 km and assign it a virtual composition of 1.0, whereas the initial mantle composition is 0.0. We then solve for the concentration field but do not consider any feedback to temperature or convective velocity, i.e. tracking the virtual composition is a post-processing step. During the thermal evolution, mobilization of the surface can lead to mixing with the mantle and a change of the virtual composition of the mantle. (Note that the surface layer concentration is always set to 1.) The effectiveness of recycling can be measured with the surface recycling factor defined as $srf = \frac{|C|-|C_0|}{|C_0|}$, where $|C_0|$ is the initial volume-averaged concentration and $|C|$ is the volume-averaged concentration after 4.5 Gyr. For instance, a value of $srf = 1$ suggests that the entirety of one surface layer volume has been recycled with the mantle during 4.5 Gyr. Large *srf* factors do not necessarily imply global and large scale resurfacing as multiple local recycling can occur at the same location but at different times. Furthermore, as a consequence of the double diffusive approach to trace the surface layer, small non-zero *srf*-values have always to be expected due to numerical virtual diffusion of the compositional field.

2.2. Surface temperature, atmospheric loss processes and outgassing

The surface temperature of Venus is obtained using the results of Bullock and Grinspoon (2001). Their model considers the variation of H_2O in the atmosphere, including associated albedo changes and cloud effects, and uses the present-day concentrations of CO_2 and SO_2 as well as the present-day luminosity. Note, that the model by Bullock and Grinspoon (2001) also calculates variations in SO_2 for constant H_2O. We consider the effect of H_2O, only.

For the determination of the surface temperature, Bullock and Grinspoon (2001) used a nongray radiative-convective atmosphere model. In the lower, convective layer the temperature decreases with height along an adiabat. The upper, radiative temperature profile depends amongst others on the effective temperature T_e, i.e. the temperature at which the planet would uniformly radiate as a black body. The effective temperature relates to the solar flux S_0 according to

$$T_e = \left(\frac{1-A}{4\sigma} S_0\right)^{1/4} \tag{11}$$

where σ is the Stefan–Boltzman constant and A the mean albedo of the planet's surface (e.g. Marshall and Plumb, 2008). Considering the variation in the luminosity of the Sun, which increased over the last 4.5 Gyr by about 40% (Gough, 1981), we obtain the surface temperature as a function of time and water concentration α_{H_2O} using the relation

$$\begin{aligned} T_0(t, \alpha_{H_2O}) &= T_0(4.5\ \text{Gyr}, \alpha_{H_2O}) \frac{T_e(t)}{T_e(4.5\ \text{Gyr})} \\ &= T_0(4.5\ \text{Gyr}, \alpha_{H_2O}) \left(\frac{S_0(t)}{S_0(4.5\ \text{Gyr})}\right)^{1/4} \end{aligned} \tag{12}$$

The surface temperature at time t is therefore calculated from the present-day surface temperature T_0 (4.5 Gyr, α_{H_2O}) taken from Bullock and Grinspoon multiplied by the ratio between the effective temperature at time t and at present. This simplified relation implies that albedo changes and cloud effects do not directly depend on luminosity. We assume a linear increase of the luminosity over time in the present study but we have verified that a more complicated functional representation of the general trend using exponential or hyperbolical functions would not affect the results in significant ways.

The surface temperature for present-day Venus by Bullock and Grinspoon (2001) depending on the atmospheric water concentration is shown in Fig. 2. It should be noted that the maximum present-day surface temperature of Venus following Bullock and Grinspoon (2001) is about 920 K (considering only variations in H_2O). According to Eq. (12), the maximum surface temperature

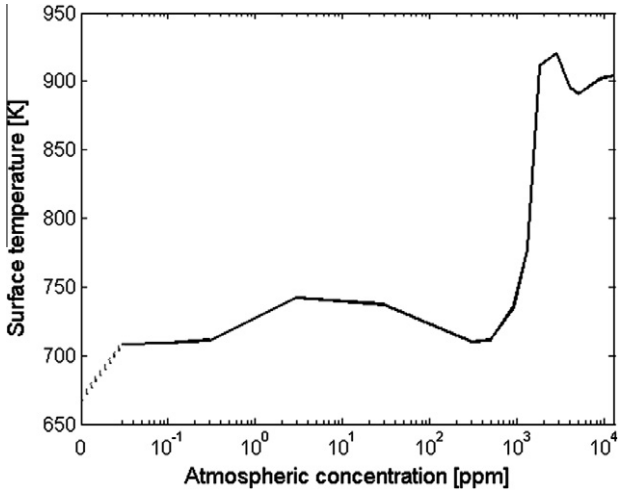

Fig. 2. Surface temperature from Bullock and Grinspoon (2001) calculated with a nongray greenhouse model of Venus under today's conditions. The surface temperature of 668 K for 0 ppmw water in the atmosphere has been taken from Taylor and Grinspoon (2009).

for early Venus would have been smaller than this value due to the lower luminosity back in time.

In addition to the outgassing from the planet interior as a source of the greenhouse gas H_2O, atmospheric loss must be considered. The exospheric escape of hydrogen is due to an electric-field flow of ions and solar wind, chemical processes like the charge exchange between hot H^+ ions and neutral hydrogen, and the collision of neutral H atoms with hot O atoms (Bullock and Grinspoon, 2001; Lewis, 2004). It can be modelled as an exponentially decreasing function of time with a characteristic lifetime τ_{H_2O}. The present-day lifetime of water τ_{H_2O} in the venusian atmosphere has been estimated between 15 and 170 Myr (Lewis, 2004; Grinspoon, 1993; Bullock and Grinspoon, 2001; Taylor and Grinspoon, 2009). However, the lifetime may have been much shorter in the early evolution of Venus due to the smaller solar luminosity (Lammer et al., 2006). For simplicity, we assume a constant lifetime of water but vary its value (15 Myr, 50 Myr and 95 Myr) to account for uncertainties.

The following equations show how the concentration of water vapour in the atmosphere is calculated over time. The time steps as well as the characteristic lifetime of water are non-dimensionalized and scaled like time in the convection model; see Eq. (4). The concentration of water at time step n (and hence its partial pressure in the atmosphere) can be calculated from the mass of water vapour ΔQ^n_{H2O} (in kg) released by extrusive volcanism in every time step k.

$$\alpha_{H_2O}(t'^n) = \alpha_{H2O,ini}\exp\left(-\frac{t^n}{\tau'_{H_2O}}\right) + \sum_{k=1}^{n}\frac{\Delta Q^k_{H_2O}}{M_{atm}}\exp\left(-\frac{t'^n - t'^k}{\tau'_{H_2O}}\right). \tag{13}$$

Here, $\alpha_{H_2O,ini}$ stands for the initial water concentration in the atmosphere and M_{atm} for atmospheric mass. Eq. (13) differs from Phillips et al. (2001) inasmuch as it considers additions to the atmospheric water inventory from all time steps. To calculate the concentration at time step n we add up additions from every prior time step multiplied by the exospheric loss function.

For very small exospheric escape times like that of water, numerical problems may arise when Eq. (13) is used for $\alpha_{H_2O}(t'^n)$. To avoid that problem, we solve Eq. (13) recursively:

$$\alpha_{H_2O}(t'^n) = \alpha_{H_2O}(t'^{n-1})\exp\left(\frac{t'^{n-1} - t'^n}{\tau'_{H_2O}}\right) + \frac{\Delta Q^n_{H_2O}}{M_{atm}}. \tag{14}$$

To obtain $\Delta Q^n_{H_2O}$, the non-dimensional mass of partial melt in the mantle is calculated from the mantle temperature at every grid point T'_i. It is widely accepted that when partial melting occurs, 1–3 wt.% of the melt are retained in the mantle (e.g. Fraeman and Korenaga, 2010); we use a value of 1 wt.% here. The remainder of the melt is immediately removed from the mantle (see also e.g. Xie and Tackley, 2004). The melt fraction is taken to increase linearly between the solidus $T_{solidus}$ and liquidus $T_{liquidus}$ and is calculated at every grid point i:

$$F'^n_{i,melt} = \max\left\{\frac{T'_i - T'_{i,solidus}}{T'_{i,liquidus} - T'_{i,solidus}} - 0.01, 0\right\}. \tag{15}$$

When the melt is removed, the solidus is increased to the current temperature in the cell volume under consideration.

The chosen solidus and liquidus curves are Earth-like and depend on pressure p. In the upper mantle (where $p < 15$ GPa), the curves are taken from de Smet (1999),

$$\begin{aligned} T_{solidus} &= 1409.15\ \mathrm{K} + 134.2\frac{\mathrm{K}}{\mathrm{GPa}}\cdot p - 6.581\frac{\mathrm{K}}{\mathrm{GPa}^2}\cdot p^2 \\ &\quad + 0.1054\frac{\mathrm{K}}{\mathrm{GPa}^3}\cdot p^3 \\ T_{liquidus} &= 2035.15\ \mathrm{K} + 57.46\frac{\mathrm{K}}{\mathrm{GPa}}\cdot p - 3.487\frac{\mathrm{K}}{\mathrm{GPa}^2}\cdot p^2 \\ &\quad + 0.0769\frac{\mathrm{K}}{\mathrm{GPa}^3}\cdot p^3 \end{aligned} \tag{16}$$

In the lower mantle (i.e. $p > 15$ GPa), we use a second-order fit of the solidus curve obtained by laboratory experiments (Zerr et al., 1998), where the solidus temperature was estimated to be about 2300 K at a pressure of 15 GPa, 3500 K at 60 GPa, and 4300 K at the CMB of the Earth. The liquidus curve is taken to be solidus-like with a temperature increased by 75 K, which corresponds to the temperature difference at 15 GPa (de Smet, 1999),

$$\begin{aligned} T_{solidus} &= 1775.74\ \mathrm{K} + 36.769\ \frac{\mathrm{K}}{\mathrm{GPa}}\cdot p - 0.134\ \frac{\mathrm{K}}{\mathrm{GPa}^2}\cdot p^2 \\ T_{liquidus} &= 1850.74\ \mathrm{K} + 36.769\ \frac{\mathrm{K}}{\mathrm{GPa}}\cdot p - 0.134\ \frac{\mathrm{K}}{\mathrm{GPa}^2}\cdot p^2 \end{aligned} \tag{17}$$

The amount of partial melt is now determined by totalling the cell volumes V'_i of the grid points i, where the solidus curve is exceeded, multiplied by the melt fraction $F'^n_{i,melt}$.

The non-dimensional quantity of water removed from the mantle at time step n is

$$\Delta Q'^n_{H_2O} = C'^n_{H_2O} C'_{extr} \sum_i V'_i(t'^n)\chi_{i,F_{melt}} \tag{18}$$

where $\chi_{i,F_{melt}}$ is one if melt occurred in grid cell i (i.e. if $F'^n_{i,melt} > 0$) and zero otherwise. The following assumptions have been made to derive Eq. (18): (1) Only extrusive volcanism can contribute to the release of volatiles. The amount of extrusive volcanism is assumed to be $C'_{extr} = 10\%$ (Crisp, 1984; Bullock and Grinspoon, 1996; Reese et al., 2007). (2) The partition coefficient of water and carbon dioxide between silicate and melt is zero, i.e. all volatiles in a partially molten cell volume are enriched in the melt. (3) The amount of water in the mantle $C'^n_{H_2O}$ decreases over time due to continuous water depletion by degassing.

As a consequence of the water depletion in the mantle, dehydration can lead to an increase of the mantle viscosity. To consider the effect of dehydration stiffening, we use the formulation by Fraeman and Korenaga (2010) and assume a viscosity increase of 100 between wet and dry mantle material. The mantle is homogeneously mixed instead of considering a depleted upper mantle (Solomatov and Zharkov, 1990). The amount of water in the mantle can then be calculated from

$$C'^n_{H_2O} := C'^{n-1}_{H_2O}\left[1 - C'_{extr}\left(\sum_i V'_i(t'^n)\chi_{i,F_{melt}}\right)/V'_{mantle}\right] \tag{19}$$

where V'_{mantle} denotes the non-dimensional volume of the entire mantle.

To obtain the surface temperature, the total amount of water vapour in the atmosphere is needed. For the 2D runs, the mass of outgassed water obtained from a 2D mantle convection model has to be scaled with

$$\Delta Q^{3D,n}_{H_2O} = \Delta Q^{2D,n}_{H_2O}\cdot\frac{4(r'^3_p - r'^3_c)}{3(r'^2_p - r'^2_c)} \tag{20}$$

while for the 3D models the calculated mass of outgassed water per time step can be directly used. After applying Eq. (14), the surface temperature can be obtained from Eq. (12).

2.3. Parameters

The parameters used for reference simulations of both setups, i.e. the coupled and the uncoupled model, are summarized in Table 1. Earth-like parameters have mostly been used to model the interior dynamics (Davies, 1999; Karato and Wu, 1993; Breuer, 2009), and Venus-like parameters were used in the atmosphere model (Phillips et al., 2001). Parameters that are unknown and/or influence the results significantly have been varied (see Table 2) and we performed in total 32 runs, i.e. we calculated 16 coupled and 16 uncoupled cases. In most runs, i.e. 26, we used 2D geometry and for 6 runs 3D geometry.

Among the varied parameters is the initial mantle temperature after accretion and core formation, which is not known, and the reference viscosity. The initial mantle temperature has been varied between 1400, 1700 and 2000 K and the reference viscosity, which depends on the mantle composition, between 10^{21} and 10^{22} Pa s. In some of the cases dehydration of the mantle has been considered, leading to higher reference viscosities with time, see Section 2.2. The initial amount of volatiles in the atmosphere has been varied as well; it is either zero or the present-day level in the venusian atmosphere of 30 ppmw (de Bergh et al., 1995; Phillips et al., 2001; Taylor and Grinspoon, 2009). We also varied the initial concentration of H_2O in the mantle from a moderate value of 50 ppmw H_2O (Morgan and Anders, 1980) to a reduced value of 20 ppmw H_2O and an increased value of 100 ppmw H_2O. The lifetime of water τ_{H_2O} has been varied as well between 15, 50 and 95 Myr (Lewis, 2004; Bullock and Grinspoon, 2001; Taylor and Grinspoon, 2009).

Table 1
Parameters used for our reference calculation of the thermal evolution of Venus.

Planetary parameters		Value
Planetary radius	r_p	6050 km
Core radius	r_c	3025 km
Reference surface temperature	T_0	737 K
Initial core temperature, 4.5 Gyr ago	$T_{c,ini}$	4000 K
Initial mantle temperature	$T_{m,ini}$	1700 K[a]
Mantle density	ρ_m	3300 kg/m^3
Core density	ρ_c	9000 kg/m^3
Surface acceleration	g	8.87 m/s^2
Specific mantle heat capacity	$C_{p,m}$	1 kJ/kg K
Specific core heat capacity	$C_{p,c}$	850 J/kg K
Thermal expansion coefficient	α_m	2×10^{-5} 1/K
Thermal diffusivity	κ_m	10^{-6} m^2/s
Dissipation number	Di	0.54
Reference viscosity (3 GPa, 1600 K)	η_{ref}	10^{21} Pa s[a]
Viscosity stress exponent	n	3.5
Activation energy	E	540 kJ/mol
Activation volume	V	15 cm^3/mol
Thermal Rayleigh number	Ra	5.288×10^7
Internal Rayleigh number	Ra_Q	3.41×10^9
Initial heat sources	H_0	7.59×10^{-8} W/m^3
Decay rate of heat sources	λ	0.0625 Gyr^{-1}
Atmosphere properties		
Present-day solar flux	S_0	2632 W/m^2
Reference mass of atmosphere	M_{atm}	4.9×10^{20} kg
Reference surface pressure	P_0	95×10^5 Pa
Present-day mixing ratio of CO_2	α_{CO2}	96.5%
Present-day mixing ratio of H_2O	α_{H2O}	30 ppmw
Transfer of volatiles		
Initial amount of volatiles H_2O in the melt	$C_{H2O,ini}$	50 ppmw[a]
Amount of extrusive volcanism	C_{extr}	10%
Initial amount of volatiles H_2O in the atmosphere	$\alpha_{H2O,ini}$	0 ppmw[a]
Lifetime of H_2O	τ_{H_2O}	95 Myr[a]

[a] These values are varied to show the robustness of our model. All parameter sets are listed in Table 2.

Table 2
List of the calculated cases (1–16) including the varied parameters. *Dim* is the geometry 2D or 3D, η_{ref} the reference viscosity, $T_{m,ini}$ the initial mantle temperature, $\alpha_{H_2O,ini}$ the initial concentration of H_2O in the atmosphere and $C_{H_2O,ini}$ the initial concentration of H_2O in the mantle, τ_{H_2O} the lifetime of H_2O, and *Dehyd.* dehydration of the mantle.

Case	Dim	η_{ref}	$T_{m,ini}$	$\alpha_{H_2O,ini}$	$C_{H_2O,ini}$	τ_{H_2O}	Dehyd.
1	2D	10^{21} Pa s	1700 K	0 ppmw	50 ppmw	95 Myr	Yes
2	2D	10^{21} Pa s	1700 K	0 ppmw	50 ppmw	50 Myr	Yes
3	2D	10^{21} Pa s	1700 K	0 ppmw	50 ppmw	15 Myr	Yes
4	2D	10^{21} Pa s	2000 K	0 ppmw	50 ppmw	15 Myr	Yes
5	2D	10^{21} Pa s	1400 K	0 ppmw	50 ppmw	15 Myr	Yes
6	2D	10^{21} Pa s	1400 K	0 ppmw	50 ppmw	95 Myr	Yes
7	2D	10^{22} Pa s	1700 K	0 ppmw	50 ppmw	95 Myr	No
8	2D	10^{21} Pa s	1700 K	0 ppmw	50 ppmw	95 Myr	No
9	2D	10^{21} Pa s	1700 K	0 ppmw	50 ppmw	50 Myr	No
10	2D	10^{21} Pa s	1700 K	0 ppmw	50 ppmw	15 Myr	No
11	2D	10^{21} Pa s	1700 K	0 ppmw	20 ppmw	15 Myr	Yes
12	2D	10^{21} Pa s	1700 K	0 ppmw	100 ppmw	15 Myr	Yes
13	2D	10^{21} Pa s	1700 K	30 ppmw	50 ppmw	95 Myr	Yes
14	3D	10^{21} Pa s	1700 K	0 ppmw	50 ppmw	95 Myr	Yes
15	3D	10^{22} Pa s	1700 K	0 ppmw	50 ppmw	95 Myr	No
16	3D	10^{21} Pa s	1400 K	0 ppmw	50 ppmw	95 Myr	Yes

The key output parameters of our calculations are listed in Table 3 for all models. These are the maximum surface velocities and surface temperatures during the entire evolution, the present-day values of the maximum surface velocity, surface temperature, the mean mantle temperature, the concentration of water in the atmosphere, the amount of water left in the mantle in ppmw and per cent, the surface recycling factor, as well as the maximal and mean surface age.

3. Results

The coupled interior and atmosphere model shows that an increase in surface temperature leads not only to an increase of partial melt in the mantle; it also strongly influences the style of mantle convection and the surface tectonic regime. In Figs. 3 and 4 we compare the coupled and uncoupled model in our reference 2D calculation (see Table 1; Case 1 in Table 2) at 2.2 Gyr. When the surface temperature reaches a critical value (which is not a constant value (Reese et al., 1999) but depends on the mantle rheology and temperature and will be discussed below) in the coupled model, convection turns from a stagnant-lid into a mobile-lid-like regime. The transition can be explained by the fact that the viscosity contrast over the upper mantle ($\eta_{surf}/\eta_{mantle}$) is locally reduced to a value smaller than about 10^5 – the viscosity contrast required for stagnant-lid convection to occur (Solomatov and Moresi, 1996). In Fig. 3b, which shows the velocity slice for the coupled model, convection cells reach the surface and mobilize it. In Fig. 4, viscosity and velocity profiles are compared for two cuts through the mantle that are indicated by white lines (A and B) in Fig. 3b. Profile A, where no mobilization of the surface occurs, shows a viscosity contrast between the smallest viscosity value to the surface value of 1.1×10^5. In profile B the contrast is only 4.2×10^4. As this does not satisfy the criterion for a stagnant-lid regime, mobilization takes place at the surface. This effect cannot be observed when the surface temperature is uncoupled from the mantle convection model, i.e. when a constant surface temperature of 737 K is applied during the evolution (Fig. 3a). The smallest viscosity contrast for the uncoupled model at 2.2 Gyr is 3.2×10^5, hence the flow remains in the stagnant-lid regime at all times and surface velocities are zero or at least very small.

In Fig. 5 we show the thermal evolution of Venus in terms of surface and mean mantle temperature, surface velocity, heat flux, and water concentration in the atmosphere and the mantle. To

Table 3
Output parameters of all models using the parameters listed in Tables 1 and 2. For each case, a coupled (Case #-c) and an uncoupled (Case #-u) model have been calculated. $v_{s,max}$ is the maximum surface velocity and $T_{0,max}$ the maximum temperature during the entire evolution, $v_{s,4.5Gyr}$ is the maximum surface velocity after 4.5 Gyr and $T_{0,4.5Gyr}$ the surface temperature after 4.5 Gyr, $\langle T_m \rangle_{4.5\ Gyr}$ is the mean mantle temperature after 4.5 Gyr, $\alpha_{H_2O,4.5Gyr}$ is the concentration of water (in a 95-bar atmosphere) after 4.5 Gyr, $C_{H_2O,4.5Gyr}$ the amount of water left in the mantle after 4.5 Gyr in ppmw and per cent, $srf_{4.5Gyr}$ is the surface recycling factor after 4.5 Gyr, Age_{max} (in Myr) is the maximum surface age and Age_{mean} is the average surface age.

Case	$V_{s,max}$ (mm/yr)	$T_{0,max}$ (K)	$V_{s,4.5Gyr}$ (mm/yr)	$T_{0,4.5Gyr}$ (K)	$\langle T_m \rangle_{4.5Gyr}$ (K)	$\alpha_{H_2O,4.5Gyr}$ (ppmw)	$C_{H_2O,4.5Gyr}$ (ppmw)	$C_{H_2O,4.5Gyr}$ (%)	$srf_{4.5Gyr}$ 1	Age_{max} (Myr)	Age_{mean} (Myr)
1-c	7.5	901	5.0	758	2962	1095	30.88	62	3.37	1578	135
1-u	0.14	916	0.13	915	2995	2176	28.49	57	0.04	2300	42
2-c	4.3	887	1.6	733	2976	854	30.00	60	1.76	2254	76
2-u	0.14	887	0.13	760	2995	1111	28.49	57	0.04	2300	42
3-c	0.93	878	0.3	711	2989	407	28.90	58	0.14	2390	37
3-u	0.14	881	0.13	710	2995	323	28.49	57	0.04	2300	42
4-c	0.2	877	0.07	737	3173	31	20.22	40	0.03	1487	266
4-u	0.07	884	0.07	737	3176	30	20.06	40	0.02	1532	231
5-c	2.0	892	1.1	723	2807	98	38.24	76	0.42	1804	147
5-u	0.17	891	0.16	718	2815	147	38.39	77	0.04	1849	97
6-c	8.7	904	8.1	744	2782	974	37.76	76	2.62	1802	108
6-u	0.16	904	0.16	733	2816	867	38.21	76	0.04	1849	118
7-c	0.96	918	0.96	915	3048	2226	25.81	52	0.10	721	78
7-u	0.01	919	0.01	916	3042	2298	25.06	50	0.007	586	44
8-c	12.8	895	8.8	715	2896	188	33.86	68	6.31	2525	219
8-u	0.37	895	0.37	713	2918	237	33.73	67	0.13	2570	231
9-c	4.8	885	3.26	724	2914	93	33.65	67	3.59	2525	243
9-u	0.37	885	0.37	721	2918	117	33.73	67	0.13	2570	242
10-c	1.84	882	1.37	738	2919	23	33.66	67	1.44	2525	251
10-u	0.38	882	0.38	738	2918	19	33.75	68	0.14	2570	223
11-c	0.05	720	0.05	720	2990	125	11.53	58	0.012	2255	17
11-u	0.13	721	0.12	721	2995	119	11.33	57	0.04	2435	18
12-c	3.1	885	1.3	716	2980	570	58.70	59	1.14	2300	61
12-u	0.13	884	0.13	720	2995	625	56.99	57	0.04	2300	41
13-c	8.1	900	5.4	750	2960	1023	30.92	62	3.43	1353	116
13-u	0.13	916	0.13	915	2995	2167	28.5	57	0.04	2300	43
14-c	6.7	896	3.5	716	2782	570	33.91	68	3.94	3247	169
14-u	0.3	911	0.2	906	2889	3421	26.73	54	0.23	454	0.4
15-c	2.1	919	2.1	917	2903	2362	23.94	48	1.34	2254	22
15-u	0.09	918	0.04	907	2910	1782	21.57	43	0.046	2254	7
16-c	7.3	903	3.2	717	2612	575	39.98	80	3.27	4510	199
16-u	0.3	899	0.2	747	2700	997	38.89	78	0.22	2706	127

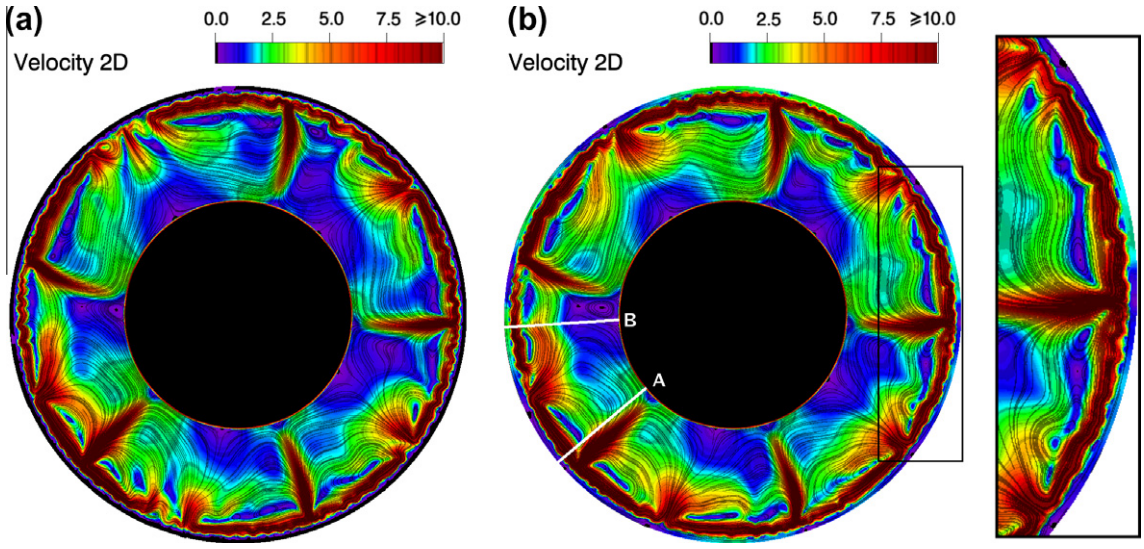

Fig. 3. Convective velocity in mm/yr for (a) the uncoupled and (b) the coupled model including a detail image for the reference case (Case 1) at 2.2 Gyr. For a better visualization of small surface velocities the values have been cut above 10 mm/yr. In the coupled case, velocities at the surface reach values of up to 2.5 mm/yr. In the uncoupled model, assuming a constant surface temperature, the surface velocity is negligible – no mobilization takes place in that model.

better understand the effect of the mobilized surface on mantle dynamics, we compare this model to the uncoupled version. After 600 Myr, partial melting first occurs and the surface temperature increases in both models (Fig. 5a). In the coupled model, the increased surface temperature insulates the mantle and results in a decrease of the heat flux (Fig. 5d). During the subsequent 1.4 Gyr an increased volcanic outgassing rate follows for both models. This fits in with the idea of the positive feedback mechanism by Phillips et al. (2001) sketched in Fig. 1. However, after 1.3 Gyr a critical surface temperature is reached for the coupled model and the surface

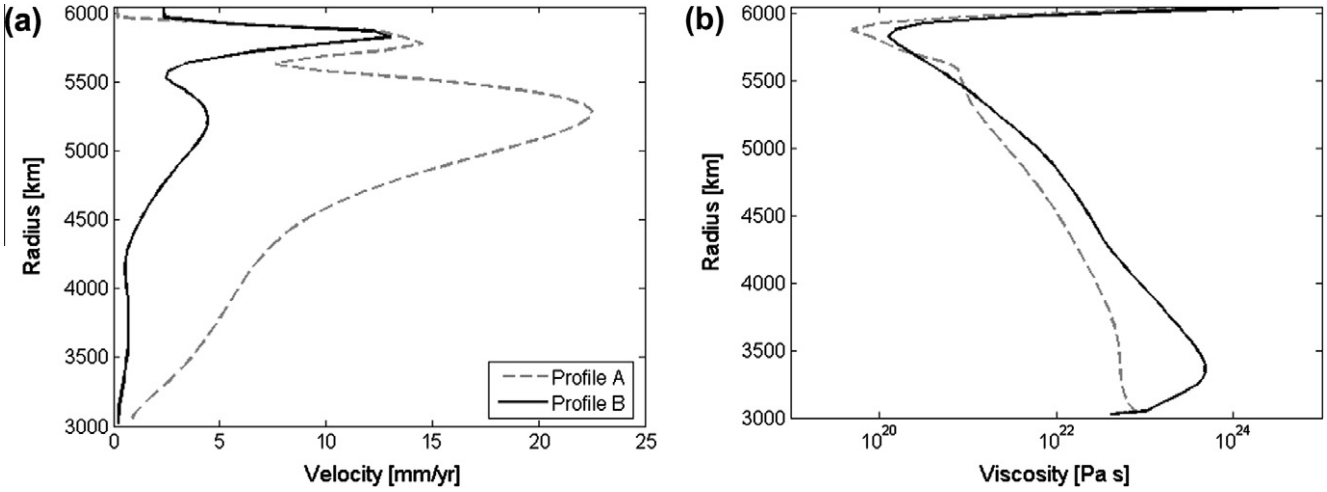

Fig. 4. Profiles of (a) velocity in mm/yr and (b) viscosity in Pa s for the reference simulation (Case 1). The profiles are cuts through the mantle, indicated by white lines in Fig. 3b. In profile A (gray dashed line) the viscosity contrast is above the limit of 10^5 Pa s for which no surface mobilization takes place. Profile B (black solid line) shows a region where the viscosity contrast is smaller and the surface is locally mobilized.

becomes locally mobilized. The maximum surface velocity increases continuously to about 7.5 mm/yr (Fig. 5c). As a result of the associated efficient cooling of the mantle, partial melting is reduced and the surface temperature decreases after about 3.5 Gyr, resulting also in a declining surface mobilization at that time. After 4.5 Gyr, the mantle is cooler in the coupled model (Fig. 5e), even though for most of the time surface temperatures have been higher than in the uncoupled model, where we assume a constant surface temperature of 737 K. The overall outgassing rate is smaller in the coupled model, so that after 4.5 Gyr less water is degassed from the mantle than in the uncoupled model (Fig. 5f).

Small fluctuations can be seen in the surface temperature during the thermal evolution (Fig. 5a). This is due to the melting model we used. If the temperature in a cell volume is higher than the solidus, partial melting occurs. The solidus increases accordingly, and the temperature has to increase further for more partial melting, which may take some time, so that there is no outgassing and surface temperature increase in certain intervals.

In the following, we show that the general findings are independent of the chosen geometry. Using 3D geometry and the same parameters as in the 2D reference case shows similar results (Fig. 6). In fact the surface mobilization as well as the cooling of the mantle is more pronounced for the coupled 3D case (Case 14 in Table 2) than for the 2D case (Case 1). For instance, at the time of mobilization the surface velocity increases more rapidly for the 3D case (Case 14-c) whereas an adjustment time of about 800 Myr has been identified for the 2D case (compare Figs. 5c and 6c). Nevertheless, the efficiency of resurfacing for the 3D case with *srf* equal to 3.94 is similar compared to the 2D reference case with a value of 3.37, see Table 3. Strong variations in the surface temperature can be observed after about 3 Gyr in the 3D case. This variation, however, is not the consequence of the 3D geometry but rather of the atmosphere model by Bullock and Grinspoon (2001). At around 1000–2000 ppmw water vapour in the atmosphere the surface temperature is very sensible to changes in the amount of atmospheric water (compare Fig. 2).

The surface of Venus is very young on average but may also contain some older parts like crustal plateaus (Phillips and Hansen, 1998). For comparison, we show the surface age obtained from our simulation with a 3D model (Case 14-c) in Fig. 7a. The age of every grid point is defined by the time at which the last partial melting occurred underneath the lithosphere. We assume that partially molten material is immediately extracted and assign its age to the surface directly above. This way we underestimate the surface age as we do not consider that a substantial amount of this melt will likely not reach the surface but remain in the crust as intrusive material. Surface age might also be altered by surface mobilization and resurfacing due to subduction-like processes but these effects on the age determination are neglected here as well. Maximum and averaged surface ages are listed in Table 3. For all cases, the averaged surface is as expected younger than the observed average venusian surface with an age of approximately 500 Myr. However, it is interesting to note that even if our averaged surface ages are smaller than the observed present-day surface age of Venus, areas can be locally quite old. These strong variations in surface age also have been observed for Venus (Hansen and López, 2010).

The surface heat flux and the surface velocity of the 3D run at 3Gyr are presented in Fig. 7b and c. Both parameters show again that mobilization is a local effect. Mantle upwellings reach the surface and increase the heat flux at these spots to 132 mW/m^2. The original surface material is shifted away from the site of the upwelling.

To demonstrate the robustness of our approach, we varied key model parameters such as reference viscosity, initial mantle temperature, exospheric loss rate for hydrogen, and initial volatile concentrations in the mantle in different simulations in 2D and 3D. Independent of the parameters used, the effects described above occurred in all cases where surface temperatures were high enough for a short time. But the critical temperature for resurfacing depends on the value of these parameters.

In Fig. 8, we show an example of how the critical surface temperature for resurfacing depends on viscosity. We used 2D simulations with the parameters given in Table 1. In all cases, the activation energy was 540 kJ/mol and the viscosity stress exponent 3.5. No partial melting or atmospheric evolution was considered in these runs, and we used fixed surface temperatures. Depending on the Peclet number, we defined four different regimes: stagnant ($Pe < 1$), highly sluggish ($1 \leqslant Pe > 10$), sluggish ($10 \leqslant Pe < 100$), and mobile ($Pe \geqslant 100$). In Fig. 8a, we compare the critical surface temperatures for the different regimes obtained for varying reference viscosities and a fixed activation volume of 10 cm^3/mol. Smaller reference viscosities lead to more vigorous convection in the mantle and lower critical temperatures. In Fig. 8b, we varied the activation volume for a fixed reference viscosity of 10^{22} Pa s and determined the dependence of the critical surface temperature on pressure effects.

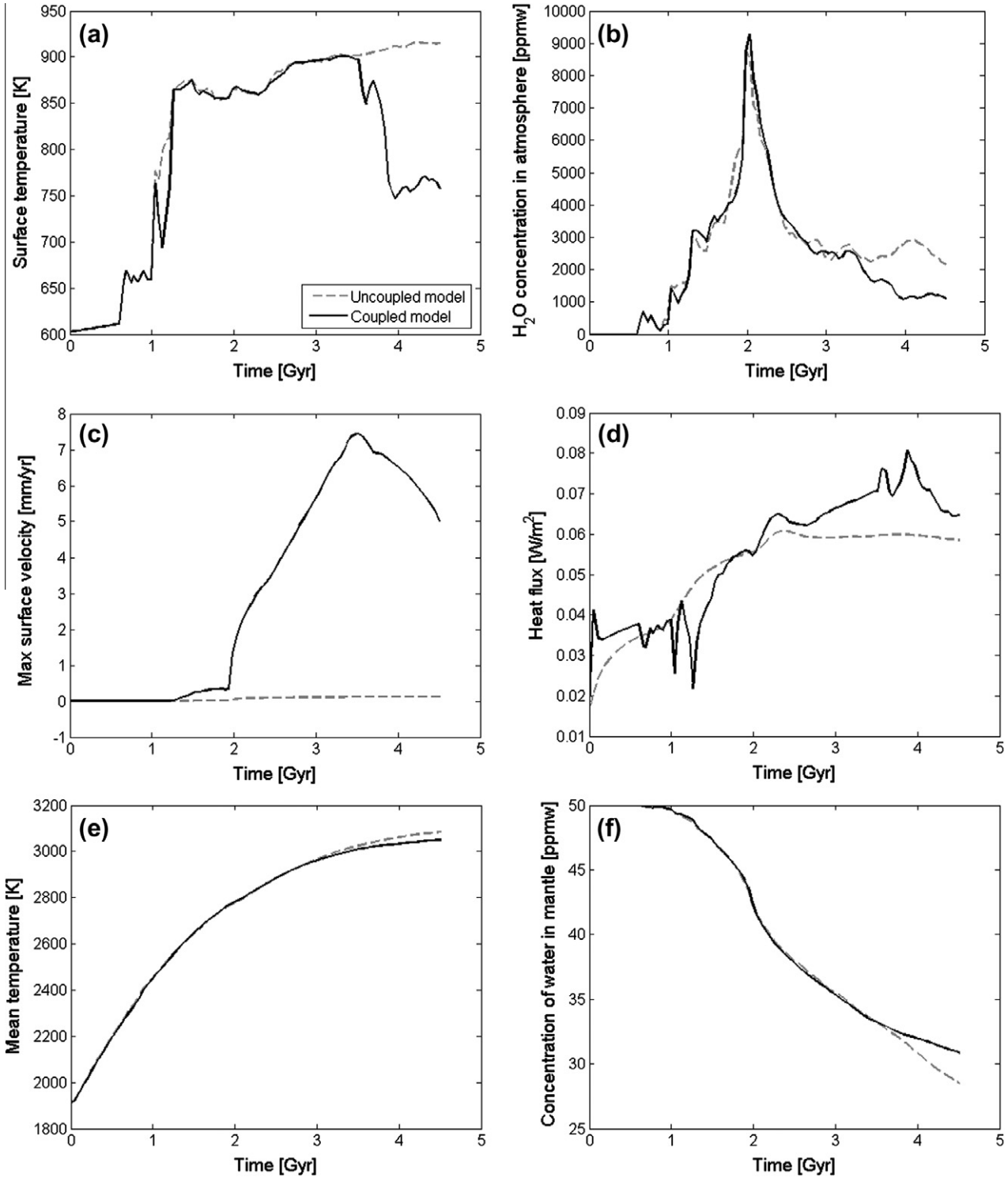

Fig. 5. (a) Surface temperature, (b) concentration of H_2O volatiles in the atmosphere, (c) maximum root-mean-square velocity of the surface material, (d) mean heat flux at the surface, (e) volume-averaged mantle temperature, and (f) amount of H_2O in the mantle as functions of time for the 2D reference model (Case 1). The black solid line indicates the coupled and the gray dashed line the uncoupled model.

We used an activation volume ranging from a small value of 2.5 cm^3/mol up to 20 cm^3/mol – the latter value is assumed for non-Newtonian fluids in the upper mantle (Karato and Wu, 1993). At high activation volumes the lower mantle becomes more sluggish and super-plumes form at the CMB. They reach the uppermost mantle and, being of greater force (due to convective stresses) than smaller plumes, they can mobilize the surface more easily. In general it can be stated that the critical surface temperature greatly depends on convective stresses and the vigour of mantle convection, which together have the effect of decreasing the viscosity contrast in the upper mantle to less than 10^5, initiating mobilization. Depending on the parameters used, critical surface temperatures range between 750 K and 1000 K.

Fig. 9 shows the theoretical dependence of the mantle temperature and rheology on the critical surface temperature, assuming that a viscosity contrast from surface to mantle lower than 10^5

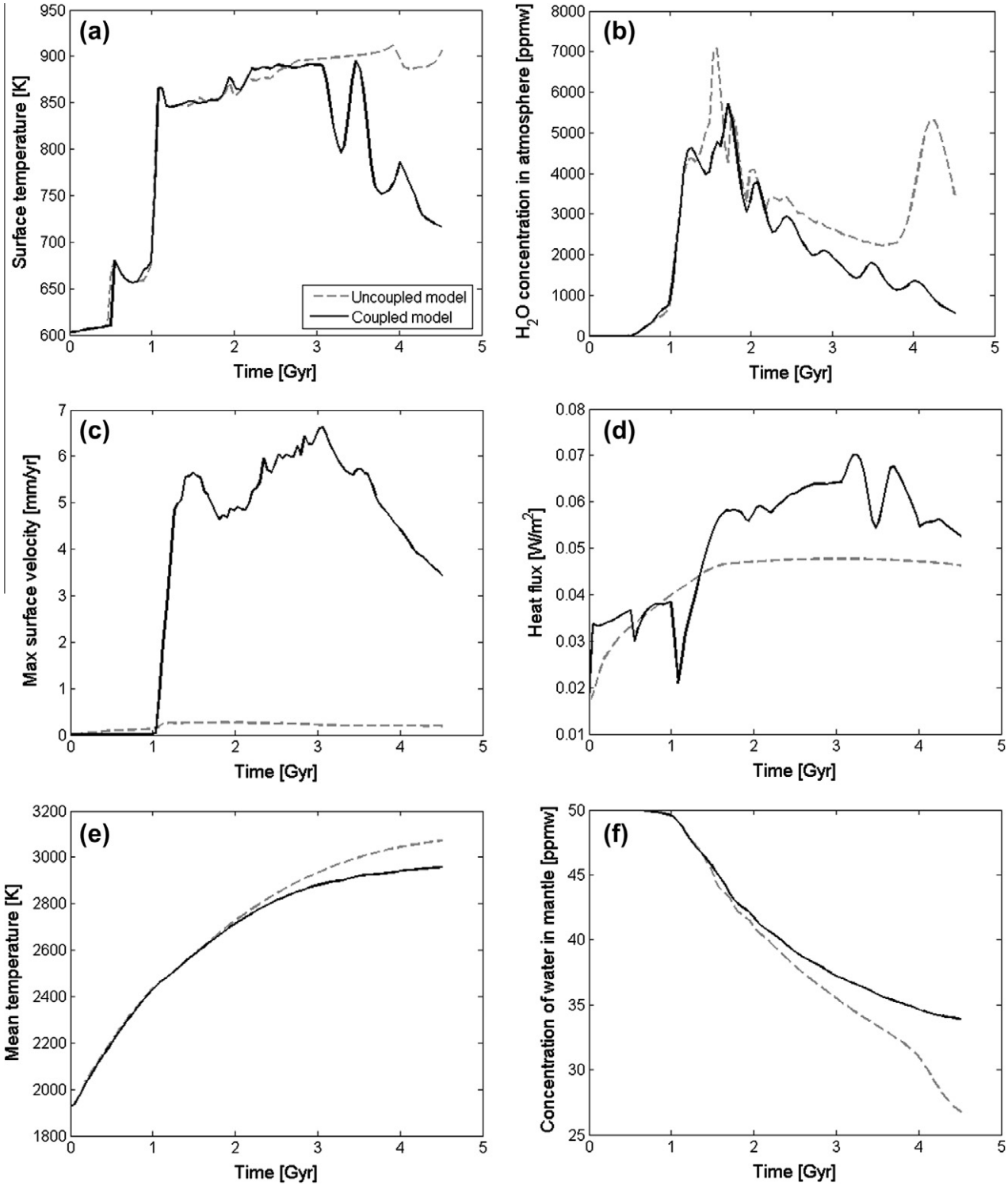

Fig. 6. (a) Surface temperature, (b) concentration of H_2O volatiles in the atmosphere, (c) maximum root-mean-square velocity of the surface material, (d) mean heat flux at the surface, (e) volume-averaged mantle temperature, and (f) amount of H_2O in the mantle as functions of time for the 3D model (Case 14). The black solid line indicates the coupled and the gray dashed line the uncoupled model.

($\eta_{surf}/\eta_{mantle} \leqslant 10^5$) is required for surface mobilization. In this approach the mantle temperature is assumed to be the temperature below the upper thermal boundary layer, and the activation volume is neglected. Three main tendencies can be observed. First, the critical surface temperature decreases with decreasing mantle temperature. Second, the critical surface temperature is lower for a non-Newtonian than for a Newtonian rheology; and third, the critical surface temperature is lower in a wet mantle. The result of the analytical solution agrees with the results shown in Fig. 8a. At smaller reference viscosities, mantle cooling is more efficient, and mantle temperatures decrease, leading to lower critical surface temperatures (cf. Figs. 8a and 9). The conclusion is that a wet and non-Newtonian mantle is more susceptible to surface mobilization. Results further indicate that the suggested surface

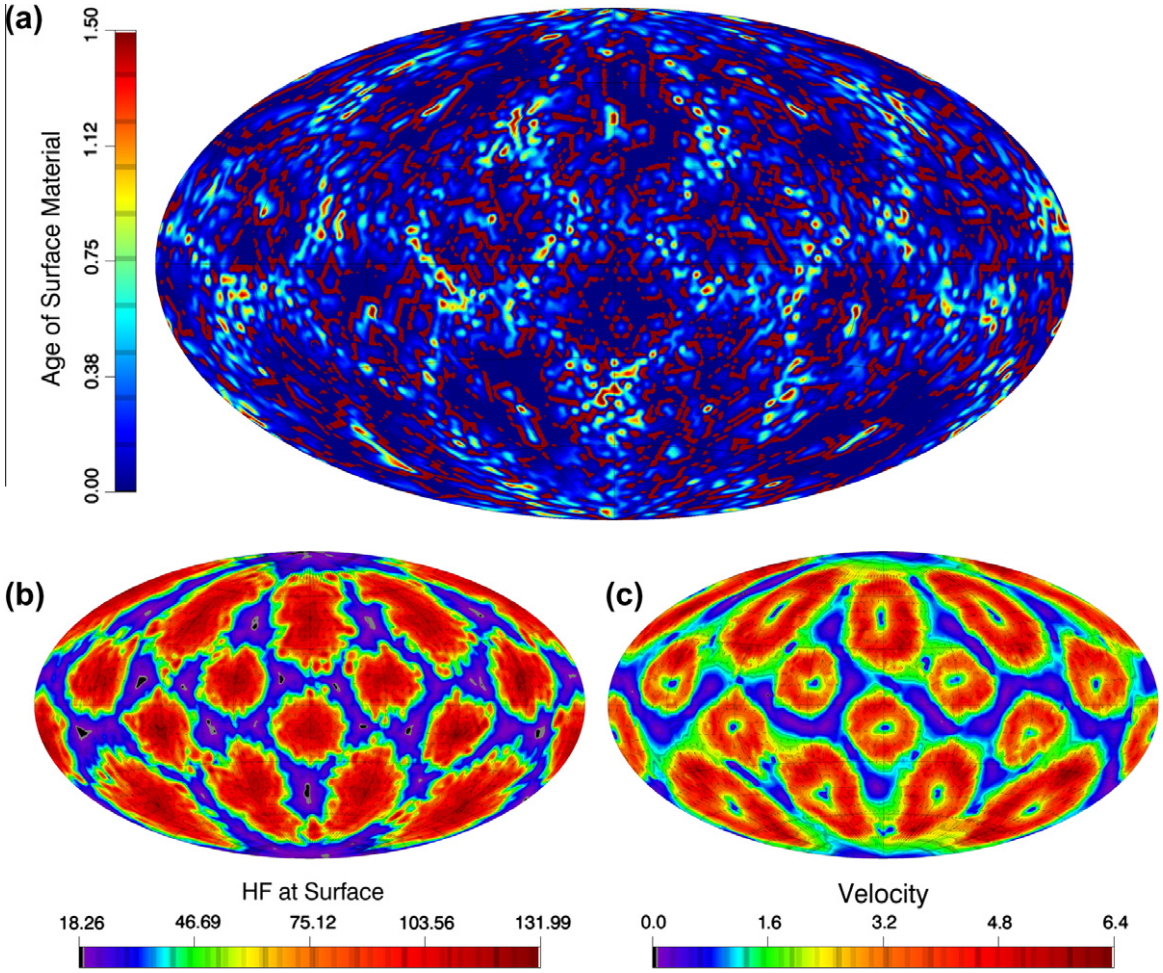

Fig. 7. (a) Age in Gyr of the surface material (Case 14-c) defined by the time at which the last partial melting occurred underneath the lithosphere – resurfacing due to mobilization is not considered (the average surface age is 169 Myr), (b) heat flux at the surface in mW/m^2 and (c) surface velocity in mm/yr at 3 Gyr.

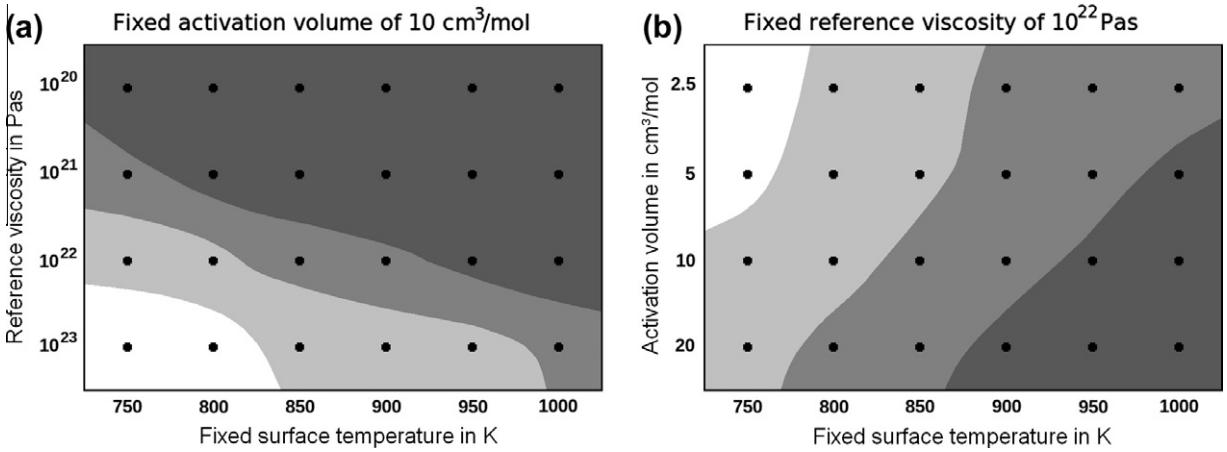

Fig. 8. Ranges of Peclet number for varying surface temperature depending on (a) reference viscosity (in Pa s) or (b) activation volume (in cm^3/mol) for a 2D simulation with a non-Newtonian fluid with constant prefactors. The dark grey area denotes regions where the Peclet number is larger than 100 (extensive surface mobilization), the lighter area denotes regions where the Peclet number is between 10 and 100 (sluggish convection), the bright gray area denotes regions where the Peclet number is between 1 and 10 (highly sluggish convection) and the white area denotes regions where the Peclet number is smaller than 1 consistent to a stagnant lid during the whole evolution.

mobilization on Venus seems to be unlikely for a Newtonian mantle rheology because this would call for surface temperatures of more than 1000 K or, alternatively, a very cool mantle.

We have shown that the critical surface temperature and, therefore, the ability to mobilize the surface depend strongly on the rheology and temperature of the mantle. Table 2 lists the simulations

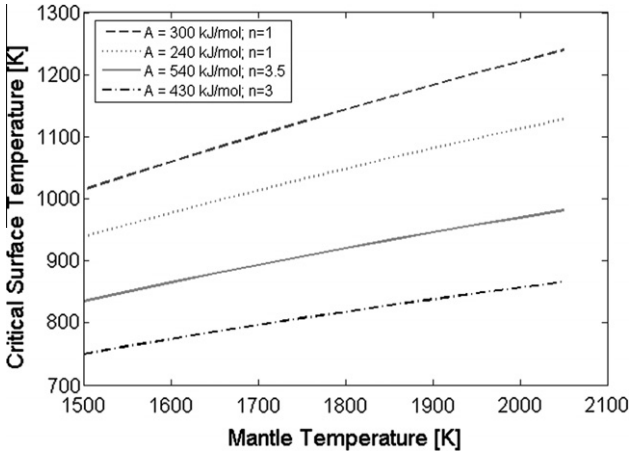

Fig. 9. Critical surface temperature as a function of mantle temperature, i.e. the temperature below the upper thermal boundary layer, for four different mantle rheologies (Karato and Wu, 1993): $A = 300$ kJ/mol and $n = 1$ (dry Newtonian rheology); $A = 240$ kJ/mol and $n = 1$ (wet Newtonian rheology); $A = 540$ kJ/mol and $n = 3.5$ (dry non-Newtonian rheology) and $A = 430$ kJ/mol and $n = 3$ (wet non-Newtonian rheology).

in which we varied these parameters as well as the initial concentrations and exospheric loss time of the greenhouse gas H_2O. We compare the coupled and uncoupled model, show how the mobilization of the surface influences interior dynamics in most of the cases investigated, and discuss the influence of different parameters on thermal evolution.

In most of the cases, the coupled model produced less outgassing: at the end of the evolution, a greater amount of volatiles remains in the mantle in the coupled (e.g. 62% in Case 1-c) than in the uncoupled model (e.g. 57% in Case 1-u). The lower average outgassing rates can be explained by surface mobilization and its cooling effect. The influence of initial mantle temperatures on the thermal evolution of Venus has been compared in Cases 5-c (1400 K), 3-c (1700 K), and 4-c (2000 K). The higher the initial mantle temperature the more efficient the degassing of the planetary interior. At $T_{m,ini} = 2000$ K, only 40% of the initial volatile content of the mantle is left after 4.5 Gyr; at $T_{m,ini} = 1400$ K, a larger proportion (76%) remains in the mantle. The maximum local surface velocity to occur during the thermal evolution decreases as initial temperatures increase – as expected (compare Fig. 9). It is 2 mm/yr at $T_{m,ini} = 1400$ K, 0.9 mm/yr at $T_{m,ini} = 1700$ K, and only 0.2 mm/yr at $T_{m,ini} = 2000$ K. This can be explained due to the fact that the decoupling of the mantle from the lithosphere becomes more pronounced as convection becomes more vigorous. At the highest initial mantle temperature investigated, 2000 K, the mean mantle temperature of the coupled model is still more than 360 K higher after 4.5 Gyr than in Case 5-c, and more than 180 K higher than in Case 3-c. High mantle temperatures lead to small mantle viscosities and hence larger viscosity contrasts to the surface than for cooler mantles. Hence the critical surface temperature to overcome is higher for the hot-mantle case than for the other two cases (see also Fig. 9).

The two extreme cases, a cold initial mantle of 1400 K (Case 5-c) and a hot initial mantle of 2000 K (Case 4-c), are compared in Fig. 10. In the hot-mantle case, extensive partial melting occurs almost from the beginning. In the cold-mantle case, almost no partial melting occurs in the first 2.5 Gyr of thermal evolution. In the hot-mantle case, already more than 40% of volatiles in the mantle have been outgassed after 2.5 Gyr compared to about 5% in the cold-mantle case at the same time. A sudden but effective volcanic event occurs shortly after the 2.5 Gyr point, releasing more volatiles than in the hot-mantle case since the mantle was not depleted

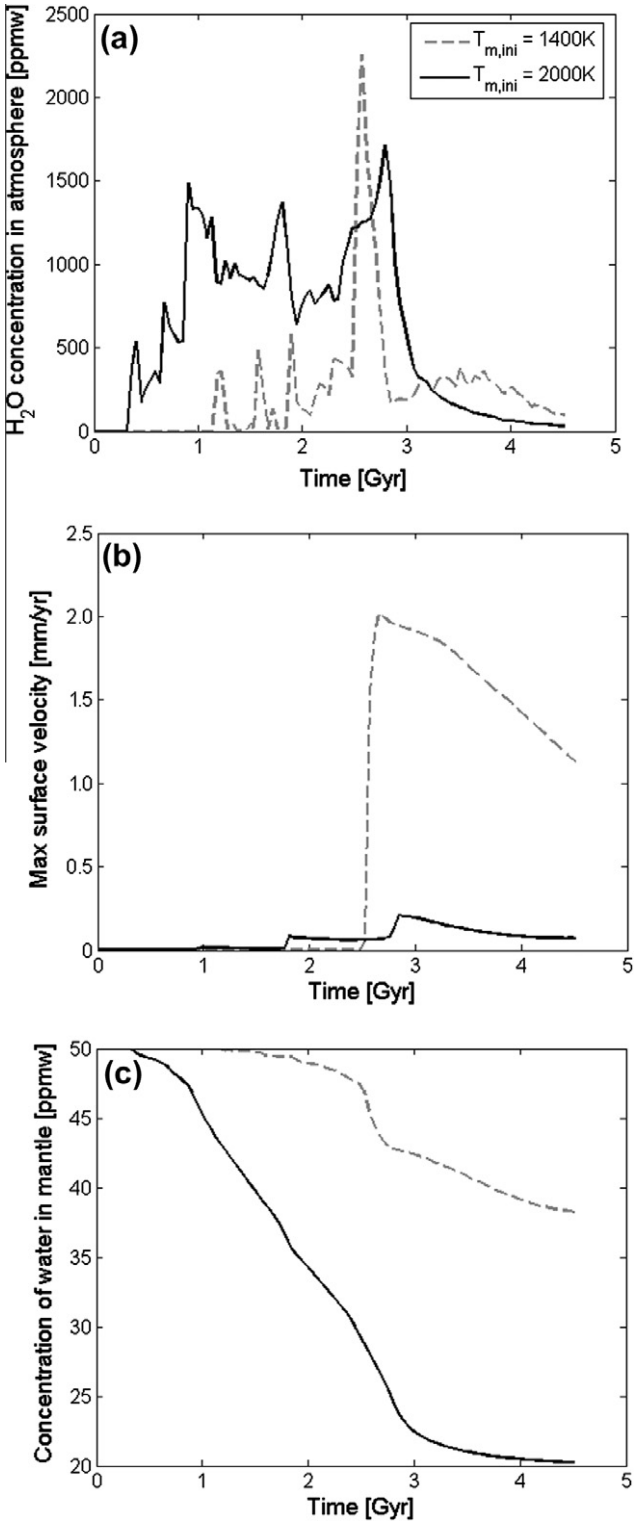

Fig. 10. (a) Concentration of H_2O in the atmosphere, (b) maximal surface velocity and (c) concentration of H_2O in the mantle as functions of time for initial mantle temperatures of 1400 K (Case 5-c) and 2000 K (Case 4-c).

of incompatible volatiles before. Surface temperatures are 20 K higher than the maximal surface temperature in the hot-mantle case, and together with the reduced viscosity contrast explained above this leads to more intense mobilization of the surface material. The hot initial mantle leads to earlier but much weaker mobilization events.

We observe the same tendency for the 3D geometry, where we compare two cases with initial mantle temperatures of 1700 K (Case 14) and 1400 K (Case 16). The latter case has a strongly reduced outgassing rate compared to the hot-mantle case. As could already be seen in the 2D investigations, a cooler mantle leads to higher maximal surface temperatures and surface velocities.

In our reference case we treated dehydration of the mantle material following Fraeman and Korenaga (2010). To investigate the effect of dehydration on our model we compare the reference case with Case 8, where no dehydration was considered. In this simulation the results are similar to the run (Case 1) shown in Fig. 5, however, after 4.5 Gyr, surface temperatures and outgassing rates are higher for the reference case. This can be explained by the stiffening of the mantle material, which leads to less effective heat transport to the surface, a warmer mantle and thus higher outgassing rates and surface temperatures. The resurfacing is more efficient in Case 8-c (with $srf = 6.31$) compared to the reference case (with $srf = 3.37$), see Table 3.

The same effect of dehydration can be observed in 3D geometry. In Case 14 the material was dehydrated during the thermal evolution, leading to high mantle viscosities after 4.5 Gyr. This case is compared to Case 15, where stiffer material was used right from the beginning of the evolution instead of considering dehydration effects. As expected, resurfacing is again less efficient for the case where stiffer material is used (with $srf = 1.34$) compared to Case 14 ($srf = 3.94$).

Stiffening of the material due to dehydration leads to reduced surface velocities and less effective surface recycling. The same tendency can be observed when using a higher reference viscosity during the whole evolution, compare Case 7 and Case 8. In both cases no dehydration of the mantle material was considered. An increase of the reference viscosity by a factor of 10 leads to more sluggish convection and hence less effective resurfacing with $srf = 0.1$ (Case 7-c) compared to $srf = 6.31$ (Case 8-c). The consequences of varying the reference viscosity have been indicated also in Fig. 8a, where the surface mobilization occurs at lower surface temperatures and is more effective when using smaller reference viscosities. Considering that smaller reference viscosities of 10^{19}–10^{20} Pa s are possible for Venus if sufficient water is in the mantle (e.g. Karato and Wu, 1993), larger surface velocities and more effective recycling than in our investigated cases (see Table 2) are possible. However, for numerical reasons we used high reference viscosities in the thermal evolution models with mantle degassing.

Hence in all simulations, maximum local surface velocities are small when compared to mantle velocities or Earth's plate velocities. The highest surface velocity in our study is 13 mm/yr in Case 8-c. The high velocities that appear in Cases 1, 6, 8, 13 and 14 were obtained because a long exospheric escape time of H_2O was assumed, leading to higher surface temperatures and velocities during the evolution. At shorter exospheric escape times (Cases 2 and 3 compared to Case 1 as well as Cases 8, 9 and 10), the amount of H_2O in the atmosphere is smaller since the loss of H_2O into space happens at a higher rate. This automatically leads to lower surface temperatures and, consequently, lower surface velocities and *srf* values.

In the following, we examine the influence of the initial concentration of volatiles in the mantle on the evolution of the atmosphere. In Cases 11 and 12 we use the same parameters as in Case 3 except initial volatile concentration vary from 20 ppmw to 100 ppmw of H_2O, respectively. Surface temperatures and velocities are smallest during the entire evolution in Case 11 with the lowest volatile content in the mantle. The surface temperature never reaches present-day temperatures, but has a maximum value of 720 K. Hence no resurfacing takes place. Surface temperatures, velocities and surface-recycling factor increase with increasing initial volatile concentration. Averaged surface ages increase with increasing volatile amount in the mantle as the mantle temperature decreases due to surface mobilization leading to less partial melt. The initial concentration of water seems to have only a minor influence on the surface temperature after 4.5 Gyr if the initial mantle water concentration is above 20 ppmw.

An initial water concentration in the atmosphere of 30 ppmw (Case 13) has almost no influence on the atmospheric evolution (compared to Case 1). Even though the initial surface temperature is higher for Case 13, the initial amount of water is rapidly lost to space.

4. Discussion

We have shown that resurfacing on Venus (which creates patches of young surface material) can be explained by a mobilization process on a planet subject to high surface temperatures. As shown in Figs. 8 and 9, surface temperature critically depends on the rheology and the mantle temperature. We find that the surface will become locally mobilized where the viscosity contrast in the mantle, i.e. the contrast between the surface and the convecting interior, falls below 10^5. At that viscosity contrast, a change from stagnant-lid convection to a transitional regime was observed in previous numerical studies (e.g. Solomatov and Moresi, 1996). Mobilization results in cooling of the upper mantle, thereby reducing degassing and tending to stop mobilization as the viscosity contrast increases again to values larger than 10^5. Note that our investigations have been done for non-Newtonian rheology parameters but with constant prefactors. First investigations involving a non-Newtonian rheology with varying strain rates show that this approximation is acceptable; viscosities at the surface can even be lower than in our approach, enhancing surface mobilization.

In the evolution models presented above, the present-day concentration of H_2O in the atmosphere is in most cases found to be higher than what is actually observed on Venus. This suggests that our present-day degassing rates are too high and would argue for even more cooling and surface recycling and thus lower outgassing rates in the recent past. One might object that exospheric loss rates may have been substantially larger than assumed during the early evolution of Venus (Lammer et al., 2006). However, since water can be seen as a short-lived greenhouse gas, the remembrance of the present-day model atmosphere for early loss rates is small to insignificant. It is possible that the venusian mantle is drier than we have assumed, possibly also due to an enrichment of volatiles in the crust.

In this work we used a simple melt model, which assumes that the solidus temperature is equal to the mantle temperature after melting. To produce new partial melting at a later stage of the thermal evolution, the mantle temperature must be increased further. This might lead to lower surface temperatures in our approach, since our melt amount might be an underestimate. On the other hand, we assumed a homogenously mixed mantle with respect to its water content. If partial melting occurs, residual water volatiles will again be extracted 100% from specific locations in the mantle, independently of previous melting. This assumption might have caused us to overestimate our outgassing rates. Overall, the two effects might compensate each other. The effect of local mantle dehydration and depletion on outgassing rates will be investigated in a future study.

In our model we did not consider that partial melting produces a buoyant crust and possibly also a buoyant depleted mantle (harzburgite) layer. These layers – if sufficiently thick – may hamper the described surface mobilization on Venus. It has been suggested for instance for early Earth that the formation of a thick basaltic oceanic crust may have had inhibited early plate tectonics (e.g.

Oxburgh and Parmentier, 1977). However, this effect can be compensated by the transition from basalt to eclogite in the lower crust for a crustal thickness of 30–70 km. This transition might enhance surface recycling, since it would lead to more dense material and a negative buoyancy of the crust (Nimmo and McKenzie, 1998). A study of these competing effects on the surface mobilization of Venus needs further consideration and is beyond the scope of the present paper.

In the present study, we used the surface temperatures derived by a model by Bullock and Grinspoon (2001) that depends on the effect of cloud layers and the resultant albedo changes. In this model they vary either H_2O or SO_2 and assume present-day concentrations of the other major greenhouse gases in the venusian atmosphere. A more realistic approximation of the venusian surface temperature with time requires the consideration of a variation in H_2O together with carbon dioxide and sulphur dioxide variations in the atmosphere. For instance, including SO_2 might lead to even higher surface temperatures as used in our model. Solomon et al. (1999) modelled a volcanic eruption with Earth-like outgassing of SO_2 and H_2O leading to a water concentration of 50 ppmw in the atmosphere and obtained an increase of surface temperature by 60 K mostly due to SO_2. Furthermore, we did not include a complete CO_2 cycle in our coupled atmosphere–mantle convection model. Such a cycle would imply carbon recycling through surface mobilization. It is not entirely clear, however, how a carbon cycle would work on Venus without abundant liquid water on the surface and without precipitation. Possibly, the cycle on Venus also includes some weathering of lava flows (Fegley et al., 1992; Zolotov and Volkov, 1992).

The main goal of this paper is, first, to show how important the feedback effects of a varying surface temperature are for the planet's interior dynamics, and second, that a change from a stagnant to a mobile-lid regime – and thus local resurfacing – may even occur at surface temperatures ranging from 750 K to 1000 K, strongly depending on rheological parameters. Since mobilization is largely independent of the atmospheric parameters chosen (see Figs. 8 and 9) it is expected that it will appear in a more realistic atmosphere model as well.

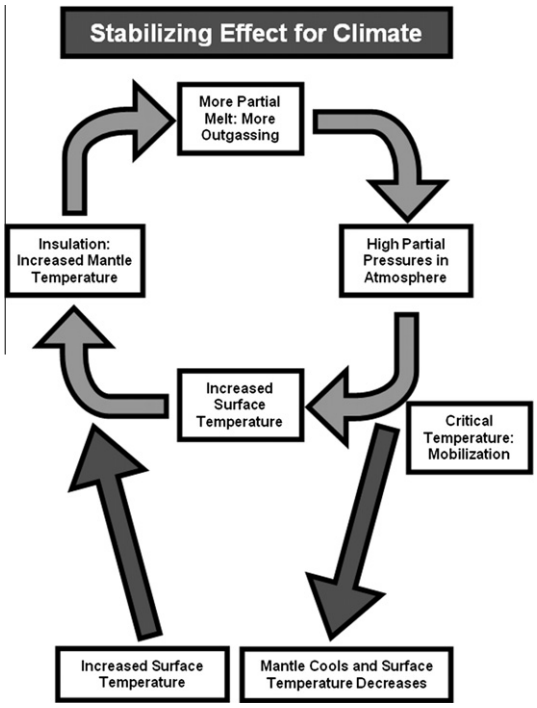

Fig. 11. Sketch indicating the climate stabilization of Venus. In contrast to the suggested runaway greenhouse mechanism shown in Fig. 1, the climate of Venus is stabilized when the surface temperatures exceed a critical limit and local surface mobilization sets in.

5. Conclusion

Our model indicates that the young surface of Venus may be explained by an increase in surface temperature by up to 150 K (relative to the present-day value). High degassing rates and the greenhouse effect cause this increase in the surface temperature and the associated surface mobilization (not plate tectonics, which would call for a cold and stiff crust), thus bringing new material to the surface. Resurfacing events appear (and disappear) self-consistently when the thermal evolution of Venus is coupled with an atmosphere model.

Local surface mobilization does not only lead to resurfacing events that may explain the surface structure and age distribution observed on Venus, it also causes an extensive decrease in mantle temperature. This is due to the lack of insulation in the lid. The amount of partial melting decreases too, leading to weaker (but still ongoing) volcanism and outgassing rates. This negative feedback mechanism regulates surface temperatures (Fig. 11) once a critical temperature is reached that can range from 750 K to 1000 K depending on rheological parameters.

The model presented in this paper shows that atmospheric changes caused by outgassing and exospheric loss processes are key elements to consider when modelling the interior of planets like Venus. These planets have the potential to reach high surface temperatures either because of their dense atmosphere or because of a high solar flux, as may be the case in most of the rocky exoplanets that have been detected so far.

Acknowledgments

This work has been performed under the HPC-EUROPA2 project (Project No. 228398) with the support of the European Commission – Capacities Area – Research Infrastructures. In addition, it was supported by the Helmholtz Association through the Planetary Evolution and Life research alliance.

We would like to thank Mark Bullock and an anonymous reviewer for their thorough and constructive reviews, which helped to improve the manuscript substantially. We would like to thank Christian Hüttig for the development of the GAIA code and Ana-Catalina Plesa for the development of the partial melt module. Furthermore, the corresponding author wishes to thank Stefano Pierini and his colleagues from Università di Napoli Parthenope for a worthwhile stay during the HPC-EUROPA2 project.

References

Basilevsky, A.T., Head III, J.W., 1998. The geologic history of Venus: A stratigraphic view. J. Geophys. Res. 103, 8531–8544.
Breuer, D., 2009. Dynamics and Thermal Evolution. Landolt-Börnstein VI-4B, Solar System, Springer, pp. 254–270.
Bullock, M.A., Grinspoon, D.H., 1996. The stability of climate on Venus. J. Geophys. Res. 101, 7521–7529.
Bullock, M.A., Grinspoon, D.H., 2001. The recent evolution of climate on Venus. Icarus 150, 19–37.
Buske, M., 2006. Three-dimensional Thermal Evolution Models for the Interior of Mars and Mercury. (Dreidimensionale thermische Evolutionsmodelle für das Innere von Mars und Merkur). PhD Thesis, Georg-August-University, Göttingen (in German).
Christensen, U.R., 1984. Convection with pressure- and temperature-dependent non-Newtonian rheology. Geophys. J. R. Astron. Soc. 77, 343–384.
Crisp, J.A., 1984. Rates of magma emplacement and volcanic output. J. Volc. Geotherm. Res. 20, 177–211.
Davies, G.F., 1999. Dynamic Earth – Plates, Plumes and Mantle Convection. Cambridge University Press.
de Bergh, C. et al., 1995. Water in the deep atmosphere of Venus from high-resolution spectra of the night side. Adv. Space Res. 15 (4), 79–88.

de Smet, J.H., 1999. Evolution of the Continental Upper Mantle. PhD Thesis. Geologica Ultraiectina, No. 172.
Fegley Jr., B., Treiman, A.H., Sharpton, V.L., 1992. Venus Surface mineralogy: Observational and theoretical constraints. Proc. Lunar Sci. Conf. 22, 3–19.
Fowler, A.C., O'Brian, S.B.G., 1996. A mechanism for episodic subduction on Venus. J. Geophys. Res. 101 (E2), 4755–4763.
Fraeman, A.A., Korenaga, J., 2010. The influence of mantle melting on the evolution of Mars. Icarus 210, 43–57.
Gough, D.O., 1981. Solar interior structure and luminosity variations. Solar Phys. 74, 21–34.
Grinspoon, D.H., 1993. Implications of the high D/H ratio for the sources of water in Venus' atmosphere. Nature 363, 428–431.
Guest, J.E., Stofan, E.R., 1999. A new view of the stratigraphic history of Venus. Icarus 139, 55–66.
Hansen, V.L., 2000. Geologic mapping of tectonic planets. EPSL 176, 527–542.
Hansen, V.L., López, I., 2010. Venus records a rich early history. Geology 38 (4), 311–314.
Hauck, S.A., Phillips, R.J., Price, M.H., 1998. Venus: Crater distribution and plains resurfacing models. J. Geophys. Res. 103, 13635–13642.
Hüttig, C., Stemmer, K., 2008. Finite volume discretization for dynamic viscosities on Voronoi grids. PEPI 171, 137–146.
Ita, J., King, S., 1994. Sensitivity of convection with an endothermic phase change to the form of governing equations, initial conditions, boundary conditions, and equation of state. J. Geophys. Res. 99 (B8), 15919–15938.
Ivanov, M.A., Head, J.W., 1996. Tessera terrain on Venus: A survey of the global distribution, characteristics, and relation to surrounding units from Magellan data. J. Geophys. Res. 101, 14861–14908.
Karato, S.-i., Wu, P., 1993. Rheology of the upper mantle: A synthesis. Science 260, 771–778.
Lammer, H. et al., 2006. Loss of hydrogen and oxygen from the upper atmosphere of Venus. Planet. Space Sci. 54 (13–14), 1445–1456.
Lenardic, A., Jellinek, A.M., Moresi, L.-N., 2008. A climate induced transition in the tectonic style of a terrestrial planet. EPSL 271, 34–42.
Lewis, J.S., 2004. Physics and Chemistry of the Solar System. Elsevier.
Marshall, J., Plumb, R.A., 2008. Atmosphere, Ocean, and Climate Dynamics – An Introductory Text. Elsevier.
McKinnon, W.B., Zhanle, K.J., Ivanov, B.A., Melosh, J.H., 1997. Cratering on Venus: Models and observations. In: Venus II. Arizona Univ. Press, pp. 969–1014.
Moresi, L.-N., Solomatov, V.S., 1998. Mantle convection with a brittle lithosphere: Thoughts on the global tectonic style of the Earth and Venus. Geophys. J. Int. 133, 669–682.
Morgan, J.W., Anders, E., 1980. Chemical composition of Earth, Venus, and Mercury. Geophysics 77 (12), 6973–6977.
Mueller, N. et al., 2008. Venus surface thermal emission at 1 μm in VIRTIS imaging observations: Evidence for variation of crust and mantle differentiation conditions. J. Geophys. Res. 113, E00B17.
Nimmo, F., McKenzie, D., 1998. Volcanism and tectonics on Venus. Annu. Rev. Earth Planet. Sci. 26, 23–51.
Noack, L., 2009. CIDGA: Coupling of Interior Dynamic Models with Global Atmosphere Models. Science and Supercomputing in Europe. HPC-Europa2 Report 2009, p. 37.
Oxburgh, E.R., Parmentier, E.M., 1977. Compositional and density stratification in oceanic lithosphere – Causes and consequences. J. Geol. Soc. Lond. 133, 343–355.
Parmentier, E.M., Hess, P.C., 1992. Chemical differentiation of a convecting planetary interior: Consequences for a one plate planet such as Venus. Geophys. Res. Lett. 19 (20), 2015–2018.
Phillips, R.J., Hansen, V.L., 1998. Geological evolution of Venus: Rises, plains, plumes, and plateaus. Science 279, 1492–1497.
Phillips, R.J. et al., 1992. Impact craters and Venus resurfacing history. J. Geophys. Res. 97, 15923–15948.
Phillips, R.J., Bullock, M.A., Hauck II, S.A., 2001. Climate and interior coupled evolution on Venus. Geophys. Res. Lett. 28 (9), 1779–1782.
Plesa, A.-C., Breuer, D., 2010. Influence of partial melt on mantle convection in a spherical shell: Application to Mars. EPSC 2010, EPSC2010-6351 (abstract).
Pollack, J.B., 1969. A nongray CO_2–H_2O greenhouse model of Venus. Icarus 10, 314–341.
Pollack, J.B., Toon, O.B., Boese, R., 1980. Greenhouse models of Venus' high surface temperature, as constrained by Pioneer Venus measurements. Geophys. Res. Lett. 85 (A13), 8223–8231.
Reese, C.C., Solomatov, V.S., Moresi, L.-N., 1999. Non-Newtonian stagnant lid convection and magmatic resurfacing on Venus. Icarus 139, 67–80.
Reese, C.C., Solomatov, V.S., Orth, C.P., 2007. Mechanism for cessation of magmatic resurfacing on Venus. J. Geophys. Res. 112, E04S04.
Romeo, I., Turcotte, D.L., 2010. Resurfacing on Venus. Planet. Space Sci. 58, 1374–1380.
Ruiz, J., 2007. The heat flow during the formation of ribbon terrains on Venus. Planet. Space Sci. 55, 2063–2070.
Sagan, C., 1969. Gray and nongray planetary atmospheres structure, convective instability, and greenhouse effect. Icarus 10 (2), 290–300.
Schaber, G.G. et al., 1992. Geology and distribution of impact craters on Venus: What are they telling us? J. Geophys. Res. 97 (E8), 13257–13301.
Schubert, G., Solomatov, S., Tackley, P.J., Turcotte, D.L., 1997. Mantle convection and the thermal evolution of Venus. In: Venus II. Geology, Geophysics, Atmosphere, and Solar Wind Environment. Springer, pp. 1245–1288.
Schubert, G., Turcotte, D.L., Olson, P., 2002. Mantle Convection in the Earth and Planets. Cambridge University Press.
Smrekar, S.E. et al., 2010. Recent hot-spot volcanism on Venus from VIRTIS emissivity data. Science 328 (5978), 605–608.
Solomatov, V.S., Moresi, L.-N., 1996. Stagnant lid convection on Venus. J. Geophys. Res. 101, 4737–4753.
Solomatov, V.S., Zharkov, V.N., 1990. The thermal regime of Venus. Icarus 84, 280–295.
Solomon, S.C., Bullock, M.A., Grinspoon, D.H., 1999. Climate change as a regulator of tectonics on Venus. Science 286, 87–90.
Stein, C., Fahl, A., Hansen, U., 2010. Resurfacing events on Venus: Implications on plume dynamics and surface topography. Geophys. Res. Lett. 37, L01201.
Steinbach, V., Yuen, D.A., Zhao, W.L., 1993. Instabilities from phase transitions and the timescales of mantle thermal evolution. Geophys. Res. Lett. 20, 1119–1122.
Stofan, E.R., Brian, A.W., Guest, J.E., 2005. Resurfacing styles and rates on Venus: Assessment of 18 venusian quadrangles. Icarus 173, 312–321.
Strom, R.G., Schaber, G.G., Dawson, D.D., 1994. The global resurfacing of Venus. J. Geophys. Res. 99, 10899–10926.
Taylor, F., Grinspoon, D., 2009. Climate evolution of Venus. J. Geophys. Res. 114, E00B40.
Turcotte, D.L., 1993. An episodic hypothesis for venusian tectonics. J. Geophys. Res. 98 (E9), 17061–17068.
Turcotte, D.L., Schubert, G., 2002. Geodynamics. Cambridge University Press.
Turcotte, D.L., Morein, G., Roberts, D., Malamud, B.D., 1999. Catastrophic resurfacing and episodic subduction on Venus. Icarus 139 (1), 49–54.
van Hunen, J., van den Berg, A.P., Vlaar, N.J., 2004. Various mechanisms to induce present-day shallow flat subduction and implications for the younger Earth: A numerical parameter study. PEPI 146, 179–194.
Wildt, R., 1966. The greenhouse effect in a gray planetary atmosphere. Icarus 5 (1-6), 24–33.
Xie, S., Tackley, P.J., 2004. Evolution of helium and argon isotopes in a convecting mantle. PEPI 146, 417–439.
Zerr, A., Diegeler, A., Boehler, R., 1998. Solidus of Earth's deep mantle. Science 281, 243–246.
Zolotov, M.Y., Volkov, V.P., 1992. Chemical processes on the planetary surface. In: Barsukov, V.L., Senior (Ed.), Venus Geology, Geochemistry, and Geophysics: Research Results from USSR. Ariz. Univ. Press, pp. 177–199.